

Bayesian Spatial Point Process Modeling for Cluster Randomized Trials

Jooyeon Lee, M.S.¹ and Evan Kwiatkowski, Ph.D.*¹

¹Department of Biostatistics & Data Science, UTHealth School of Public Health, Houston, TX, USA,

*Corresponding author: Evan.K.Kwiatkowski@uth.tmc.edu

Abstract

Cluster randomized trials (CRTs) offer a practical alternative for addressing logistical challenges and ensuring feasibility in community health, education, and prevention studies, even though randomized controlled trials are considered the gold standard in evaluating therapeutic interventions. Despite their utility, CRTs are often criticized for limited precision and complex modeling requirements. Advances in robust Bayesian methods and the incorporation of spatial correlation into CRT design and analysis remain relatively underdeveloped. This paper introduces a Bayesian spatial point process framework that models individuals nested within geographic clusters while explicitly accounting for spatial dependence. We demonstrate that conventional non-spatial models consistently underestimate uncertainty and lead to misleading inferences, whereas our spatial approach improves estimation stability, controls type I error, and enhances statistical power. Our results underscore the value and need for wider adoption of spatial methods in CRT.

Keywords: Cluster randomized trial; Bayesian; Mixed-effects model; Gaussian process, INLA

1 Introduction

Randomized controlled trials are represented as the gold standard in evaluating healthcare interventions [1]. However, in many clinical and public health studies, randomizing individuals is often impractical due to the logistical complexity of delivering interventions or the risk of contamination among the individuals. Additionally, an individually randomized controlled trial may be unacceptable to the local population, which could threaten a trial's successful completion and its social and scientific value that is essential to its justification [2–4]. More importantly, for research intended to inform policy reform, cluster randomized designs may provide findings that generalize better to real-world policy contexts [5].

In such cases, cluster randomized trials (CRTs) can provide a robust alternative in which the interventions are randomized by groups of individuals, either by geography or institution to evaluate the effectiveness of interventions. CRTs have become a fundamental design in evaluating interventions in community health, education, and health service delivery and have been a recurrent theme in clinical trial designs with methodological research devoted to matched paired designs, intraclass correlation coefficient (ICC), and appropriate sample size calculations to address issues of clustering and power [6]. Examples of CRTs in health care include primary care clinics of hospitals [7, 8], schools or community-based programs, clinical decision support systems for mental health training [9, 10], and regional vaccination campaigns [11–13].

Parallel CRTs are the most common clinical trial design that randomizes clusters to one of two or more arms [14]. The randomizing unit in this design is a cluster, so all individuals in each cluster receive only one kind of treatment during the study, usually starting simultaneously. There are several methods for analyzing parallel CRTs. In a case where cluster sizes are equal and in a two-arm trial, a simple way is to use a two-sample t-test to compare cluster-level mean responses between the groups. When there are more than two treatment arms, a one-way analysis of variance may be useful. In a special case, where a matched-pairs design is used, a paired t-test can be conducted. When cluster sizes are unequal, individual-level analysis such as random effects models [15] or generalized estimating equations (GEE) [16] may be used.

A defining feature of CRTs is the intraclass correlation coefficient (ICC), which quantifies the degree of similarity in outcomes among individuals within the same cluster. A high ICC implies that individual responses are highly correlated, which must be accounted for in both the design and analysis stages. Ignoring ICC can lead to underpowered studies and inflated type I error rates. Standard analytic strategies include mixed-effects models, which explicitly model within-cluster correlation through random effects, and GEE, which accounts for within-cluster correlation via a specified working correlation structure [17]. The Consolidated Standards of Reporting Trials (CONSORT) [18] statement provided reporting guidelines for CRTs to include ICCs for each primary outcome and account for the design effect induced by ICC in sample size calculations.

Bayesian methods in CRTs allow the incorporation of external evidence by using substantive prior opinions on key parameters, such as treatment effects, cluster-level variances, and intraclass correlations. They also provide a flexible framework for modeling hierarchical structures and capturing dependence among responses or random effects. In addition, uncertainty

about model assumptions can be directly incorporated into power calculations. Spiegelhalter (2001) [19] showcased Bayesian approaches for CRTs with continuous responses and highlighted that considerable development of robust strategies for Bayesian modeling in CRTs is still needed. A methodological systematic review of Bayesian methods in CRTs noted the lack of application of Bayesian methods relative to frequentist approaches and underscored the need for further Bayesian methodological developments in both the design and analysis of CRTs [20].

Geographic clusters are the most commonly chosen randomization unit for trials in which subgroups or entire populations are targeted for intervention testing [17]. Examples include insecticide bed-net distribution [21–24], water sanitation programs [25], vector-control interventions [26, 27], vaccination/health campaigns [28, 29], and vaccine effectiveness [30], where outcomes in neighboring areas are inherently correlated. Especially in vaccine trials, spatial dependency often arises from indirect protection mechanisms such as herd immunity [31] or human mobility patterns [32]. A systematic review of spatial CRTs [33] discussed that the incorporation of spatial effects in CRTs is rare and called for further development and evaluation of spatial methodologies across a range of CRT designs. There have been a few attempts to quantify the importance of spatial dependency in trials through spatial correlation [34] and spatial lag models [35]. Guo and Zhang (2019) [36] extended the trial design to account for spatial variation through a Bayesian adaptive design using an area-level conditional autoregressive prior.

While CRTs have received considerable attention in the literature, most of the work has not incorporated spatial considerations in design or analyses, even though the need for spatial modeling arises naturally in many cluster-based interventions. Spatially structured CRTs are particularly important when outcomes or treatment effects vary over space due to underlying geographic heterogeneity in environmental exposures, health system infrastructure, socioeconomic context, or other unmeasured confounders. To our knowledge, no published work has explored the design of CRTs that leverage point-referenced participant addresses.

In this paper, we propose a Bayesian spatial point process method in CRTs that accommodates spatial variation of participants' geocoded locations and individual-level biomarkers, characteristics, and neighborhood factors. The objective of the proposed method is to assess whether the intervention treatment is superior to the control. We account for both the cluster-specific variations and spatial variation, where we introduce a Gaussian process with geostatistical structure for spatial dependency. There are two families of methods to analyze CRTs: cluster-level analysis and individual-level analysis. Our proposed method adopted an individual-level approach that accounts for spatial structure. We compared this model with individual and cluster-level models that ignore spatial effects, evaluating performance using metrics such as power, false positive rate, percent relative error, mean squared error, bias, and coverage rate for the treatment effect.

In Section 2, we present a Bayesian point process method for treatment efficacy trials and its potential use in CRTs with continuous responses. Section 3 outlines data generation, prior specification, operating characteristics, and introduces nonspatial comparison methods to compare the performance with our proposed method. The results for the simulations are given in Section 4, while Section 5 describes the advantages and disadvantages of the methods

covered in this paper. Additional details are provided in the Supplementary Materials.

2 Methods

2.1 CRT design and Gaussian process

We assume that a larger value is preferred for continuous outcomes. Consider a two-arm CRT, where $z_i \in \{0, 1\}$ for cluster i denotes the treatment arm—control and intervention, respectively. Let \mathcal{I} denote the set of cluster regions and let $|\mathcal{I}| = I$ be the number of clusters. Each cluster $i \in \mathcal{I}$ indexed by $i = 1, \dots, I$ consists of J individuals indexed by $j = 1, \dots, J$. Thus, the total number of participants in the trial is $N = IJ$. Since we are conducting a cluster randomized trial (CRT), in which randomization occurs at the cluster level by definition, we assume that all individuals within a given cluster are assigned to the same arm—either intervention or control. This design choice is consistent with best practices in CRTs, which helps prevent contamination between arms and simplifies trial implementation [17].

We specifically consider the geographical type of cluster, which could be based on administrative units, arbitrary geographic zones, or institutional clusters such as schools, health units, or workplaces. Let Y_{ij} denote the continuous outcome for the individual j in cluster i , located at spatial coordinate $\mathbf{s}_{ij} \in \mathcal{B}_i \subset D$, where a global spatial domain of the trial is denoted by $D \subset \mathbb{R}^2$ and \mathcal{B}_i is the spatial region associated with cluster $i \in \mathcal{I}$.

For any finite set of spatial locations $\{\mathbf{s}_{ij} : i = 1, \dots, I; j = 1, \dots, J\}$, if the outcome vector $\mathbf{Y} = (Y_{11}, \dots, Y_{1J}, \dots, Y_{I1}, \dots, Y_{IJ})'$ follows a multivariate normal distribution with mean vector $\boldsymbol{\mu} = (\mu_{11}, \dots, \mu_{1J}, \dots, \mu_{I1}, \dots, \mu_{IJ})'$ and covariance matrix $\boldsymbol{\Sigma}$, then the collection $\{Y(\mathbf{s}_{ij}) : \mathbf{s}_{ij} \in D\}$ is a spatial stochastic process and is said to be a Gaussian process (GP). The generic element of $\boldsymbol{\Sigma}$ is defined by a covariance function $C(\cdot, \cdot)$ such that $\Sigma_{(ij),(i'j')} = \text{cov}(y(\mathbf{s}_{ij}), y(\mathbf{s}_{i'j'})) = C(\mathbf{s}_{ij}, \mathbf{s}_{i'j'})$ [37, 38]. We assume the covariance function to be weakly stationary, in which the covariance between outcomes depends only on the distance between locations.

A hierarchical mixed-effects model incorporating within-cluster variance σ_W^2 and between-cluster variance σ_B^2 is considered to account for individual-level and cluster-level variability in CRTs and is well described in Hayes and Moulton (2009) [17]. Between-cluster variance can arise for two reasons. First, participants chosen for the cluster are often nonrandomly selected, which can create intracluster variation of the response. Second, even without the presence of selection bias, the shared experience within a cluster can cause intracluster outcome variation. This variability between clusters is extraneous to the treatment effect [5].

We extended unobserved variability to the spatial domain using a geostatistical model where the residual is partitioned into two components: a spatially structured Gaussian process and an independent random noise term. The latent spatial component captures underlying spatial patterns that are not explained by cluster-specific effects or random noise. The geostatistical structure is well formulated in spatial statistics [39].

2.2 Proposed method: CRT-SMM

We introduce a CRT spatial mixed-effects model (CRT-SMM) that offers a novel application of spatial modeling in the context of cluster randomized trials, which accounts for both between-cluster variance and geostatistical correlations. We assumed that geostatistical correlation is shared across the entire region of interest, thus the outcome Y_{ij} , observed at spatial location \mathbf{s}_{ij} , is modeled using a mixed-effects framework continuously defined over a spatial domain $D \subset \mathbb{R}^2$, and is formulated as

$$Y(\mathbf{s}_{ij}) = \mu_{ij} + u_i + w(\mathbf{s}_{ij}) + \epsilon_{ij}, \quad (1)$$

where μ_{ij} is an individual-level mean structure that accounts for cluster-level treatment indicator $z_i \in \{0, 1\}$; and a vector of K individual-specific covariates $\mathbf{x}_{ij} = (x_{ij0}, x_{ij1}, \dots, x_{ij(K-1)})'$ such as demographic, socioeconomic, or biomarker status. The covariate term x_{ij0} is set as 1 to reflect an intercept. The individual-level mean structure μ_{ij} is defined as follows:

$$\mu_{ij} = \beta z_i + \mathbf{x}'_{ij} \boldsymbol{\gamma} + z_i \cdot \mathbf{x}'_{ij} \boldsymbol{\delta}, \quad (2)$$

where β is a fixed treatment-specific effects, $\boldsymbol{\gamma} \in \mathbb{R}^K$ is a fixed covariate effects, and $\boldsymbol{\delta} \in \mathbb{R}^K$ is a fixed effects interaction term between treatment and individual-specific covariates that accounts for treatment effect heterogeneity. Note that the cluster-specific treatment indicator z_i is used instead of the individual-level z_{ij} since randomization was conducted at the cluster level and the trial was analyzed under the intention-to-treat (ITT) principle.

In this model, u_i denotes a cluster-specific random effect that is assumed to independently and identically (i.i.d.) follow a normal distribution with mean zero and has between-cluster variance σ_B^2 . ϵ_{ij} is an individual-level random noise that is assumed to i.i.d. follow a normal distribution with mean zero and within-cluster variance σ_W^2 . Spatial random effects denoted by $w(\mathbf{s}_{ij})$ are defined over individual-level spatial locations \mathbf{s}_{ij} . The three components u_i , ϵ_{ij} , $w(\mathbf{s}_{ij})$ are assumed to be mutually independent of each other.

The collection of spatial effects $\{w(\mathbf{s}_{ij}) : \mathbf{s}_{ij} \in D\}$ is assumed to follow a zero-mean Gaussian Process (GP) with covariance function:

$$\text{cov}(w(\mathbf{s}_{ij}), w(\mathbf{s}_{i'j'})) = \tau^2 \cdot \rho(\mathbf{s}_{ij}, \mathbf{s}_{i'j'}),$$

where τ^2 is the marginal spatial variance and $\rho(\cdot, \cdot)$ is an isotropic decay function that depends only on the distance between locations.

Marginalizing over the spatial effects $w(\mathbf{s}_{ij})$, the resulting covariance structure of the outcome vector is:

$$\text{cov}(\mathbf{Y}) = \boldsymbol{\Sigma} = \tau^2 \mathbf{H}(\phi) + \sigma_B^2 \mathbf{C}' \mathbf{C} + \sigma_W^2 \mathbf{I},$$

where $\mathbf{I} \in \mathbb{R}^{N \times N}$ is an identity matrix; $\mathbf{C} = \{C_{ij}\}_{i=1, \dots, I; j=1, \dots, J} \in \mathbb{R}^{I \times N}$ is a cluster membership matrix with elements C_{ij} which is a binary indicator denoting whether individual j belongs to cluster i ; and $\mathbf{H}(\phi) \in \mathbb{R}^{N \times N}$ is the correlation matrix with element (p, q) given by $H_{pq}(\phi) = \rho(\mathbf{s}_p, \mathbf{s}_q)$, where $p \mapsto (p \bmod I; p \bmod J) = (i, j)$ and $q \mapsto (q \bmod I; q \bmod J) = (i', j')$. Two common choices for the correlation function are the exponential function $H_{pq}(\phi) =$

$\exp(-\|\mathbf{s}_p - \mathbf{s}_q\|/\phi)$ and the Matérn function $H_{pq}(\phi) = (1/(2^{\nu-1}\Gamma(\nu)))(\|\mathbf{s}_p - \mathbf{s}_q\|/\phi)^\nu K_\nu(\|\mathbf{s}_p - \mathbf{s}_q\|/\phi)$, where ϕ is the decay parameter that controls the reach of spatial distance, ν is a shape parameter for smoothness, Γ is the gamma function, and function $K_\nu(\cdot)$ is the ν -order modified Bessel function of the second kind. Note that each row of \mathbf{C}' contains a one in the column corresponding to the cluster that the individual belongs to, and zeros elsewhere. Thus, the term $\sigma_B^2 \mathbf{C}' \mathbf{C}$ represents a block-diagonal covariance structure which has shared variance of individuals within the same cluster but zero covariance structure between individuals in different clusters; e.g., matrix \mathbf{C}' and $\mathbf{C}' \mathbf{C}$ for clusters $i = 1, 2, 3$ with individuals $j = 1, 2$ are as follows:

$$\mathbf{C} = \{C_{ij}\}_{i=1,\dots,I; j=1,\dots,J} = \begin{bmatrix} 1 & 1 & 0 & 0 & 0 & 0 \\ 0 & 0 & 1 & 1 & 0 & 0 \\ 0 & 0 & 0 & 0 & 1 & 1 \end{bmatrix}, \quad \mathbf{C}' \mathbf{C} = \begin{bmatrix} 1 & 1 & 0 & 0 & 0 & 0 \\ 1 & 1 & 0 & 0 & 0 & 0 \\ 0 & 0 & 1 & 1 & 0 & 0 \\ 0 & 0 & 1 & 1 & 0 & 0 \\ 0 & 0 & 0 & 0 & 1 & 1 \\ 0 & 0 & 0 & 0 & 1 & 1 \end{bmatrix}.$$

The correlation between patients within a cluster, defined as the intracluster correlation coefficient (ICC), is crucial in CRT as we assume the outcomes of patients are not independent. A review of ICC in CRTs is well described in [40]. The ICC defined in a model with spatial dependency is

$$\text{ICC} = \frac{\sigma_B^2}{\sigma_B^2 + \tau^2 + \sigma_W^2}.$$

The resulting marginal likelihood for all individuals in the study is defined through N -dimensional outcome vector \mathbf{Y} , where $N = IJ$. The outcome vector follows a multivariate normal distribution as follows:

$$\mathbf{Y}|\boldsymbol{\zeta} \sim \text{MVN}(\boldsymbol{\mu}, \tau^2 \mathbf{H}(\phi) + \sigma_B^2 \mathbf{C}' \mathbf{C} + \sigma_W^2 \mathbf{I}), \quad (3)$$

where the mean vector is specified as

$$\boldsymbol{\mu} = \mathbf{z}\beta + \mathbf{X}\boldsymbol{\gamma} + \text{diag}(\mathbf{z}) \cdot \mathbf{X}\boldsymbol{\delta} \quad (4)$$

and $\boldsymbol{\zeta} = \{\beta, \boldsymbol{\gamma}, \boldsymbol{\delta}, \tau^2, \phi, \sigma_B^2, \sigma_W^2\}$. The elements in the treatment assignment vector $\mathbf{z} \in \mathbb{R}^{N \times 1}$ contain binary indicators for each individual, where z_{ij} is 1 if individual j in cluster i is assigned to the intervention, and 0 if assigned to control group. In a CRT framework, the elements of \mathbf{z} are identical for all individuals within the same cluster, which means $z_{ij} = z_i$ for all j in cluster i . Thus, while the notation \mathbf{z} is defined at the individual level, its values reflect cluster-level randomization. $\mathbf{X} \in \mathbb{R}^{N \times K}$ is a matrix of K individual-level covariates; $\boldsymbol{\gamma}, \boldsymbol{\delta} \in \mathbb{R}^{K \times 1}$ are main effects of covariates and treatment-covariate interaction effects, respectively.

CRT-SMM can be summarized by adopting the recast of a geostatistical specification to a hierarchical form from [41]:

$$\begin{aligned} Y_{ij}|\beta, \boldsymbol{\gamma}, \boldsymbol{\delta}, \mathbf{u}, \mathbf{w}(\mathbf{s}), \sigma_W^2 &\sim N(\mu_{ij} + u_i + w(\mathbf{s}_{ij}), \sigma_W^2) \\ \mathbf{w}(\mathbf{s})|\tau^2, \phi &\sim GP(\mathbf{0}, \tau^2 \mathbf{H}(\phi)), \end{aligned} \quad (5)$$

where $\mathbf{w}(s_{ij})$ denotes the realization of a latent spatial process $\mathbf{w}(s) \in \mathbb{R}^{N \times 1}$ at the location s_{ij} of individual j in cluster i . The spatial process $\mathbf{w}(s)$ is modeled as a zero-mean Gaussian process with covariance structure governed by range parameter ϕ and marginal variance τ^2 .

We are interested in evaluating the intervention by testing the hypothesis

$$H_0 : \theta \leq \Delta \text{ vs. } H_1 : \theta > \Delta, \quad (6)$$

where θ is an overall (i.e., marginal) treatment effect denoted by the difference of the treatment arms and Δ is a minimum clinically important difference (MCID). Specifically, $\theta = \mu_1 - \mu_0$, with the population-average (i.e., marginal) treatment effect estimator defined as

$$\begin{aligned} \hat{\mu}_1 &= E[y_{ij}|z_i = 1] = \hat{\beta} + E[\mathbf{x}_{ij}|z_i = 1]'(\hat{\gamma} + \hat{\delta}) \\ \hat{\mu}_0 &= E[y_{ij}|z_i = 0] = E[\mathbf{x}_{ij}|z_i = 0]'\hat{\gamma}, \end{aligned}$$

where each of μ_0 and μ_1 represents the expected treatment response measure in the control and intervention arms, respectively. When the covariates are centered within each arm or cluster, then θ is simplified to $\theta = \beta$ which captures the average treatment effect, free from the influence of covariates.

In the Bayesian framework, a closed form of the posterior cannot be derived from our proposed model (2) due to the hierarchical structure and the presence of the spatially correlated Gaussian process (GP) prior. Moreover, the Markov chain Monte Carlo method (MCMC) requires matrix inversion of the GP covariance matrix Σ , leading to computational complexity. We thereby adopted Integrated Nested Laplace Approximation (INLA) [42] by leveraging the stochastic partial differential equations (SPDE) approach [43] and obtained posterior approximates for efficacy θ .

3 Simulation

3.1 Data generation

We conducted simulation studies to evaluate the operating characteristics of CRT-SMM in comparison with nonspatial methods—CRT-FM-naïve, CRT-FM, CRT-MM, and CRT-cluster which will be introduced in section 3.4—under realistic CRT scenario settings. For simplicity, we considered one continuous biomarker covariate in a two-arm trial. As mentioned in section 2.1, we assumed that the intervention and control were each allocated exclusively within their respective clusters in each randomization. Allocating treatments exclusively within clusters is more approachable in the real world and reduces the costs of the trial. This design reflects the defining feature of cluster randomization, where groups or clusters are randomized to treatment arms.

In our simulation, we focused on a 1:1 geographical randomization scheme to ensure an acceptable overall balance in treatment allocation. For CRTs, it is generally recommended to have highly restrictive randomization balanced on individual-level covariates or cluster-level when there is a limited number of clusters [44, 45]. Geographic balance is especially important

to reduce the likelihood that observed differences are driven by spatial heterogeneity, such as urban versus rural settings or localized outbreaks. For our simulation studies, we implemented a randomization approach that allocates clusters to treatment arms while maintaining spatial balance across the study region.

In real-world CRTs, especially within the National Cancer Institute’s Community Oncology Research Program (NCORP), estimated ICCs that are theoretically valid ranged from 0 to 0.50 [46]. Although many trials assume ICC to be less than or equal to 0.10, [46] highlighted the importance of assuming ICC to go beyond 0.10 if a robust calculation of sample size is to be made. Additionally, in trials for primary (general practitioners) and secondary care (hospital-based outpatient or inpatient settings), ICC ranged from 0.05 to 0.15 [47–49]. Other trials reported ICCs to be between 0.01 and 0.02 in human studies [50, 51].

To reflect this range of plausible real-world values, we assumed $\text{ICC} \in \{0.05, 0.15, 0.25\}$ in our simulation study to cover both conservative and higher-end ICC scenarios in practice. We considered 6 different combinations of scenarios covering true treatment effect $\theta \in \{0 - 1.4 \text{ by } 0.1\}$. Table 1 shows scenarios we considered for each model. Note that for a chosen ICC, σ_B^2 and τ^2 are calculated such that each explains 50% of the variability attributable to $\sigma_B^2 + \tau^2$. We considered a cluster size (i.e., number of participants in each cluster) of $m = 40$, a desired treatment effect of $\theta = 0.6$, and $\sigma_W^2 = 2.25$. Although the required number of clusters differed for each ICC—17, 39, and 61 for each $\text{ICC} \in \{0.05, 0.15, 0.25\}$, respectively—we fixed the number of clusters at 16 across all scenarios to isolate and evaluate the effects of spatial components independent of the number of clusters. The number of clusters in our simulations reflects real-world CRTs, where the median number of clusters has been reported as 21 in a random sample of 300 published trials [52].

We generated synthetic CRT datasets under the assumptions of a target treatment effect $\theta = 0.6$, desired power of 0.85, and type I error rate of 0.05. Data generating mechanisms based on the specified fixed effects, variance components, and ICC values are outlined below:

- Step 1. Specify fixed effects: We set the covariate effect $\gamma = 0.1$, the interaction effect $\delta = 0.1$. Covariates were simulated from $N(0, 1)$ and marginal treatment effect simplifies to $\theta = \beta$, where we set treatment effect to vary from 0 to 1.4 in increments of 0.1.
- Step 2. Define variance components: We fixed the individual-level variance $\sigma_W^2 = 2.25$ to reflect that our target treatment effect has moderate effect size $\theta = 0.4\sigma_W$. For each specified ICC, we partitioned variability attributable to $\sigma_B^2 + \tau^2$ using a proportion $f = \sigma_B^2 / (\sigma_B^2 + \tau^2)$. The between-cluster variance σ_B^2 and spatial variance τ^2 were computed as

$$\sigma_B^2 = \frac{\sigma_W^2}{\frac{1}{\text{ICC}} - \frac{1}{f}}, \quad \tau^2 = \frac{(1 - f)\sigma_B^2}{f},$$

where we set $f = 0.5$ in our simulation, allocating equal variability to the cluster-level and spatial random effects.

- Step 3. Incorporate spatial structure: We consider ICC values $\text{ICC} \in \{0.05, 0.15, 0.25\}$, which determine the corresponding σ_B^2 and τ^2 values through variance partitioning in Step 2.

The spatial decay parameter ϕ was set to either 1.5 or 3.5, chosen relative to the unit size of the simulated grid.

Step 4. Set sample size: 16 clusters (grid size 4×4) and $m = 40$ individuals per cluster are considered. This setting corresponds to the target effect size as $\theta = 0.6$, desired power 0.85, with type I error rate 0.05. The required sample size per arm to achieve this setting is calculated as

$$N = 2 \frac{\sigma_W^2 (Z_{1-\beta} + Z_{\alpha/2})^2}{\theta^2} \text{Deff},$$

where clustering is captured through design effect $\text{Deff} = 1 + (m - 1) \cdot \text{ICC}$ [6, 53]. The total number of clusters is then obtained as $2N/m$, given equal allocation to treatment and control arms. In a sample size calculation, design effect differs by the specific design (e.g., crossover, parallel, stepped-wedge) and study outcome types (e.g., continuous, binary). In our simulation, we use the specific case of parallel CRTs with a continuous outcome [54].

Step 5. Assign treatment: Clusters were allocated to treatment or control in a 1:1 ratio randomly.

Step 6. Generate outcomes: For each individual, outcomes were generated as a combination of treatment and covariate effects, cluster-level random effects, spatial random effects, and individual noise. We specifically simulated from a Gaussian random field with exponential covariance function.

3.2 Prior specification

Throughout our simulation, we utilized a novel informative Penalized Complexity (PC)-prior proposed by Simpson et al. (2017) [55], as PC-priors are suited for constructing latent effects, invariant to reparameterization, connected to Jeffreys' priors, and robust regarding the choice of user defined parameter flexibility which is straightforward to apply through INLA. PC-prior distributions are constructed on four principles:

Principle 1. Occam's razor: the prior favors the simpler base model (e.g., no random effect or no spatial effect) by penalizing deviations of more complex model.

Principle 2. Measure of complexity: the Kullback-Leibler divergence (KLD) [56]

$$\text{KLD}(\pi(\mathbf{y}|\eta) || \pi(\mathbf{y}|\eta_0)) = \int \pi(\mathbf{y}|\eta) \log \left(\frac{\pi(\mathbf{y}|\eta)}{\pi(\mathbf{y}|\eta_0)} \right) d\mathbf{y}$$

quantifies the additional complexity of a flexible model relative to the base model, that has parameters η and η_0 , respectively. The interpretable unidirectional distance between two models can then be expressed as $d(\eta) = \sqrt{2\text{KLD}(\pi(\mathbf{y}|\eta) || \pi(\mathbf{y}|\eta_0))}$.

Principle 3. Constant rate penalization: by penalizing deviation over a distance, it implies exponential prior on the distance scale, $\pi(d) = \lambda e^{-\lambda d}$, where λ is rate parameter. This corresponds to PC-prior distribution

$$\pi_d(\eta) = \lambda e^{-\lambda d(\eta)} \left| \frac{\partial d(\eta)}{\partial \eta} \right| \quad (7)$$

by change of variables rule.

Principle 4. User-defined scaling: the rate parameter λ is calibrated through an interpretable tail probability $P(Q(\eta) > U) = \alpha$, where $Q(\eta)$ is a parameter of interest, U is a user-defined upper boundaries of tail event, and α is the weight we put on. From this principle, the user can prescribe how informative the PC-priors are to be.

From the illustrated principles, the PC-prior for the variance component of a Gaussian random effect is $\pi_d(\sigma) = \lambda \exp(-\lambda \sigma)$, since the base model is assumed to be $\sigma = 0$ and the distance is defined as $d(\sigma) = \sigma$. When the user specifies tail probability $P(\sigma > U) = \alpha$, this induces an exponential prior $\sigma \sim \text{Exp}(\lambda = -\log \alpha/U)$. In other words, the PC-prior for individual-level variance, cluster-level variance, and spatial marginal variance is

$$\pi_d(\sigma_W) = \lambda e^{-\lambda \sigma_W}, \quad \pi_d(\sigma_B) = \lambda e^{-\lambda \sigma_B}, \quad \pi_d(\tau) = \lambda e^{-\lambda \tau},$$

respectively.

The PC-prior on the spatial range parameter ϕ , the base model is a flat field ($\phi \rightarrow \infty$) with distance $d(\phi) = 1/\phi$. The resulting prior is

$$\pi_d(\phi) = \lambda \phi^{-2} e^{(-\frac{\lambda}{\phi})},$$

where the rate λ is calibrated through a user-defined flexibility $P(\phi < \phi_0) = \alpha$.

We specified weakly informative priors to allow the data to dominate inference while ensuring computational stability. However, for CRT-FM which is introduced in section 3.4, can suffer from perfect multicollinearity due to the inherent structure of CRT. Thus, we specified a strongly informative prior. Common priors were used across all models unless otherwise noted.

Common priors on regression coefficients for the treatment effect and covariates $(\beta, \gamma_k, \delta_k)$ were assigned weakly informative independent normal distributions $N(0, 1000)$. The individual-level variation σ_W^2 was assigned a PC-prior $\pi_d(\sigma_W)$ with weakly informative $P(\sigma_W > 10) = 0.1$, shrinking towards smaller values while permitting larger variances if strongly supported by the data. Such a prior is consistent with the intuition of being "weakly informative" as it balances fidelity in strong signals while shrinking weak signals [55].

For model-specific priors, between-cluster variance σ_B^2 was given a PC-prior $\pi_d(\sigma_B)$ with $P(\sigma_B > 3) = 0.1$, shrinking towards smaller values while permitting larger variances if strongly supported by the data. Spatial random effects in CRT-SMM were modeled using the SPDE approach with PC-priors on the range (ϕ) and marginal variance τ^2 , assuming an exponential covariance function. We set weakly informative $\pi_d(\phi)$ with $P(\phi < 7) = 0.5$ and

$\pi_d(\tau)$ with $P(\tau > 3) = 0.1$, encouraging moderate spatial dependence but allowing flexibility for stronger or weaker spatial dependencies.

The choice of weakly informative priors aligns with standard practice for CRT analyses, where little to moderate external information is available. In the Bayesian context, however, incorporating a well-justified informative prior can add value to statistical analysis and may be considered when appropriate [20]. In our study, we utilized PC-priors on the standard deviation of the cluster-level and spatial variability, given the fact that the PC-prior is computationally efficient in fitting Bayesian hierarchical models in INLA [55].

3.3 Operating characteristics

The posterior probability of the treatment effect being greater than the MCID can be approximated as

$$Pr(\hat{\theta} > \Delta | \mathbf{D}) \approx \frac{1}{M} \sum_{m=1}^M 1[P_{H_0}(\hat{\theta}^{(m)} > \Delta)] \quad (8)$$

where \mathbf{D} is data accumulated at the end of the trial, M is the number of posterior samples drawn from marginal treatment effects, and $\hat{\theta}^{(m)}$ is a m^{th} posterior sample. In Bayesian clinical trial design, the false positive rate (FPR) and power cannot be obtained analytically because the posterior is not in a closed form. Thus, we adopt a traditional (frequentist-like) FPR and power calculation in a Bayesian trial setting. In our analysis, we used INLA, a method for approximate Bayesian inference, where the marginal posterior distribution $Pr(\hat{\theta} > \Delta | \mathbf{D})$ is approximated numerically rather than averaged from MCMC samples.

For each scenario, $S = 10,000$ number of trials were simulated, and depending on the decision boundary $1 - \alpha$, overall FPR and power are calculated. In our simulation, we chose $\Delta = 0$ for simplicity. The overall FPR which is the probability of falsely declaring meaningful efficacy is calculated as

$$\text{FPR} = \frac{\text{Number of falsely rejecting } H_0}{\text{Number of simulations } (S)}, \quad (9)$$

where falsely rejecting H_0 is denoted as $P_{\theta=0}(\hat{\theta} > \Delta | \mathbf{D}) > 1 - \alpha$. The overall power which is the probability of correctly identifying the meaningful efficacy is calculated as

$$\text{Power} = \frac{\text{Number of correctly rejecting } H_0}{\text{Number of simulations } (S)} \quad (10)$$

where correctly rejecting H_0 is denoted as $P_{\theta>0}(\hat{\theta} > \Delta | \mathbf{D}) > 1 - \alpha$.

The percent relative error (%RE), which is an informative performance measure that represents under or over-prediction [57], is calculated as

$$\%RE = \left(\frac{\text{modSE}}{\text{empSE}} - 1 \right) \times 100\%, \quad (11)$$

where modSE refers to the model-derived posterior standard error obtained from each simulation, while empSE denotes the empirical standard error calculated from the distribution of mean estimates across repeated simulations. A large positive %RE indicates that the estimate intervals are too wide (i.e., conservative), whereas a large negative %RE indicates the intervals are too narrow (i.e., anti-conservative). When the uncertainty of an estimate is underestimated, the power and type I error rate become inflated because it becomes easier to reject the null hypothesis. Also, this leads to under-coverage of the true parameter value.

Bias and mean squared error (MSE) were used to evaluate estimator performance across repeated simulations. For a true treatment effect θ and its posterior mean estimate $\hat{\theta}$ from each simulation, the bias is defined as

$$\text{Bias} = \frac{1}{S} \sum_{i=1}^S (\hat{\theta}_i - \theta) \quad (12)$$

which calculates the average deviation of the expected posterior estimates from the true value across S replicates. A bias reflects systematic error and the value that is close to zero indicates that the estimator's expected value well covers the true value. MSE is a metric of estimator accuracy defined as the sum of its variance and squared bias defined as

$$\text{MSE} = \frac{1}{S} \sum_{i=1}^S (\hat{\theta}_i - \theta)^2. \quad (13)$$

Coverage probability was used to assess the posterior uncertainties. For each simulation replicate, 95% credible interval for the treatment effect θ was constructed. Coverage probability is defined as the proportion of replicates in which the true value θ is covered by a corresponding credible interval.

3.4 Comparison methods

We considered a set of models to evaluate the impact of incorporating spatial effects in clinical trials. In our simulation, we created a single individual-specific covariate for simplicity. We compared CRT-SMM with four nonspatial methods applied to simulated CRTs. (i) naïve fixed effects model (CRT-FM-naïve), which ignores the cluster effect entirely, (ii) fixed effects model (CRT-FM), which accounts for the cluster effect as a fixed term, (iii) mixed effects model (CRT-MM), which accounts for the cluster effect as a random term, and (iv) cluster-level analysis (CRT-cluster). Across individual-level models (i)-(iii), we used the same individual-level mean structure,

$$\mu_{ij} = \beta z_i + \mathbf{x}'_{ij} \boldsymbol{\gamma} + z_i \cdot \mathbf{x}'_{ij} \boldsymbol{\delta}$$

as defined in equation (2), and included individual-level variation $\epsilon_{ij} \sim N(0, \sigma_W^2)$. For cluster-level model (iv), we used the averaged mean structure

$$\bar{\mu}_i = \beta z_i + \bar{\mathbf{x}}_i' \boldsymbol{\gamma} + z_i \bar{\mathbf{x}}_i' \boldsymbol{\delta}.$$

CRT-FM-naïve

First, we consider the CRT naïve fixed effects model (CRT-FM-naïve)

$$Y_{ij}|\beta, \gamma, \delta, \sigma_W^2 \sim N(\mu_{ij}, \sigma_W^2), \quad (14)$$

where we completely ignore the term for cluster-level variability. This is a “complete pooling” modeling approach, which completely ignores the unobserved heterogeneity in response, where it may lead to inefficient estimation, biased inference, and underestimated standard errors, resulting in spuriously inflated statistical power and type I error [58, 59]. These issues are anticipated to ultimately increase the risk of drawing incorrect conclusions about the treatment effectiveness. However, we included this model as a benchmark to assess how ignoring cluster-level variability might affect overall performance and potentially lead to incorrect conclusions about the true treatment effect.

CRT-FM

Next, we consider the CRT fixed-effects model (CRT-FM), where the effects of clusters are considered unknown but fixed. In CRTs, treatments are distributed at a cluster-level and the participants in that cluster receiving the same treatment results in unobserved heterogeneity, which means that the response will be affected by the unmeasured cluster-level factors [59]. Therefore, we included dummy cluster membership indicators with unknown fixed effects to absorb all the between-cluster variations [59] formulated as follows:

$$Y_{ij}|\beta, \gamma, \delta, \sigma_W^2 \sim N(\mu_{ij} + \xi_{g(i)}, \sigma_W^2), \quad (15)$$

where the cluster-specific fixed effects $\xi_{g(i)}$ maps each observation to its corresponding cluster $g(i) \in \{1, 2, \dots, I\}$. $\xi_{g(i)}$ can be expressed as a linear combination $\sum_{k=2}^I \xi_k \cdot \mathbb{I}\{g(i) = k\}$, where the first cluster is treated as the reference group and $\mathbb{I}\{\cdot\}$ is an indicator function denoting cluster membership. Excluding the reference group ensures identifiability of the model parameters by avoiding perfect multicollinearity among the dummy variables. This expression of fixed effects in analyzing clustered data aligns with the formulation described by Tutz and Oelker (2017) [60].

However, in parallel CRTs, treatment does not vary within clusters, which means individuals are either all treated with control or intervention. This leads CRT-FM to suffer from perfect multicollinearity, which leads to difficulty in distinguishing between the treatment effect β and cluster effect $\xi_{g(i)}$, particularly when analyzed under an intention-to-treat (ITT) framework. To partially mitigate this identifiability issue, we assigned moderately informative normal priors $N(0, 1)$ to all fixed effects, which stabilized estimation while avoiding excessive shrinkage. The CRT-FM model was included in our comparison to demonstrate its tendency to produce unstable treatment effect estimates under CRT.

CRT-MM

We consider the CRT mixed-effects model (CRT-MM) that accounts for the unobserved heterogeneity by incorporating cluster-level random effects, or random intercept, u_i . The formula for CRT-MM is as follows:

$$Y_{ij}|\beta, \gamma, \delta, \mathbf{u}, \sigma_W^2 \sim N(\mu_{ij} + u_i, \sigma_W^2). \quad (16)$$

CRT-Cluster

We also compared our models analyzed with cluster-level summary measures rather than individual-level to provide the ground for simplicity.

$$\bar{Y}_i | \beta, \gamma, \delta, \sigma_W^2 \sim N(\bar{\mu}_i, \sigma_W^2), \quad (17)$$

where $\bar{\mu}_i = \beta z_i + \bar{\mathbf{x}}_i' \gamma + z_i \bar{\mathbf{x}}_i' \delta$. In a cluster-level analysis, cluster-level covariates can be used directly instead of aggregating individual-level covariates \mathbf{x}_{ij} to $\bar{\mathbf{x}}_i$. In real-world studies, using known cluster-level variables is often more appropriate and interpretable. However, in our simulation study, we used the average of individual-level covariates within each cluster to simplify the comparison across methods.

4 Results

A total of 10,000 simulations were conducted for each scenario using R (version 4.3.3) [61]. Figure 1 is a single simulation replicate across scenarios when true treatment effect is $\theta = 0.5$, under a checkerboard restricted randomization of clusters. Although our simulation assigns treatments randomly, we present an example with a checkerboard structure to better illustrate the distribution of individual responses across treatment groups. The individual responses are generated on a 4×4 grid, where the correlation between the centers of the farthest diagonal (from the upper left to the lower right) is given by $\exp(-3\sqrt{2}/\phi)$. For example, scenarios A, C, E have a correlation of $\exp(-3\sqrt{2}/1.5) = 0.059$, and scenarios B, D, F have a correlation of $\exp(-3\sqrt{2}/3.5) = 0.297$ at the maximum grid-center distance. The figure demonstrates that within each treatment group, individuals in close proximity tend to have similar response values, whereas those farther apart show greater differences. This spatial dependency becomes more prominent as the ICC and spatial range ϕ increase.

Table 2 summarizes 10,000 simulation posterior mean estimates $\hat{\theta}$ and standard deviation $\hat{\sigma}_\theta$ for true treatment values $\theta \in \{0, 0.3, 0.6\}$ under scenarios A-F. When $\theta = 0$, all methods produced unbiased estimates, but their variance behavior differed. CRT-FM-naïve consistently underestimated uncertainty, with very small standard deviations in scenarios A-C and only modest increases in scenarios D-F. CRT-FM provided unbiased estimates with somewhat larger standard deviations, partially correcting the underestimation. CRT-MM and CRT-cluster also produced unbiased means, but their variances escalated sharply with stronger spatial correlation, reaching as high as 5.69 and 6.33 in scenario F. In contrast, CRT-SMM achieved unbiased estimates with moderate and stable variances (0.24–0.96) across all scenarios.

When $\theta = 0.3$ or $\theta = 0.6$, CRT-FM-naïve remained relatively unbiased but underestimated variance. CRT-FM, CRT-MM, and CRT-cluster showed relatively biased estimates and became severely biased under scenario F, with CRT-MM and CRT-cluster exhibiting high uncertainty ranging 1.83-5.69 and 2.00-6.34, respectively, in scenarios D-F. Meanwhile, CRT-SMM produced unbiased estimates with well-calibrated and stable variance across scenarios.

Figure 2 displays power curves from 10,000 simulations across true treatment effects θ under scenarios A-F. CRT-FM-naïve generally achieved the highest power across scenarios, although CRT-SMM surpassed it in scenarios B and D as θ increased. CRT-FM performed worst in scenario A but maintained moderate power in scenarios B-F. CRT-MM achieved

higher power when the spatial range parameter was $\phi = 1.5$ compared to $\phi = 3.5$ but its performance was substantially lower than that of CRT-SMM, unless ICC was low as 0.05. CRT-cluster followed a trend similar to CRT-MM. Our proposed method, CRT-SMM, approached the highest power levels when $\phi = 3.5$ as θ increased. It is important to note that the trial design fixed the number of clusters at 16 across all scenarios, slightly fewer than the 17 clusters suggested by sample size calculations to achieve 85% power and a type I error rate of 0.05 when the target treatment effect is $\theta = 0.6$, under ICC = 0.05. Although CRT-SMM did not surpass other methods in power at $\phi = 1.5$, its upward trend suggested that it would eventually outperform other methods once the number of clusters is optimized for higher ICC values.

The false positive rates (FPR; i.e., rejection rates when $\theta = 0$) in Figure 3 show that CRT-FM-naïve had the highest FPR ranging from 0.2 to 0.4, which represents an unacceptably inflated type I error rate. CRT-FM achieved an acceptable FPR close to 0.05 only in scenario A, but exhibited similarly inflated rates as CRT-FM-naïve in scenarios B-F. In contrast, CRT-MM, CRT-SMM, and CRT-cluster maintained acceptable FPRs across all scenarios (A-F).

Percent relative error (%RE) provides a measure of the inaccuracy of estimates relative to the true value. Figure 4 displays %RE from 10,000 simulations across all scenarios. CRT-FM-naïve exhibited the largest negative values, ranging from -45 to -90, indicating anti-conservative confidence intervals that led to inflated power, consistent with the power curves in Figure 2. CRT-FM showed slightly positive values in scenario A but similarly large negative values (-45 to -90) in scenarios B-F, reflecting the inflated power curves in Figure 2, except in scenario A where it yielded the lowest power across values of θ 's. CRT-MM produced near-zero %RE in scenarios A-C, with slightly negative values in scenarios D-F. CRT-cluster showed near-zero %RE in scenarios A-E but has a positive value of approximately 15 in scenario F. Importantly, CRT-SMM maintained %RE values consistently near zero across all scenarios (A-F), demonstrating the most reliable and well-calibrated performance among all methods.

Additional figures (Figure S1, S2, S3) present the coverage probability of θ , bias, and MSE of 10,000 simulations across all scenarios. The results show that CRT-MM, CRT-cluster, and CRT-SMM consistently achieved coverage probabilities close to 1 in all scenarios (A-F), whereas CRT-FM-naïve and CRT-FM exhibited substantially lower coverage, with the exception of CRT-FM attaining the highest coverage in scenario A. The complete pooling approach (CRT-FM-naïve) in Figure S2 demonstrates that failure to account for unobserved heterogeneity induces additional bias [62, 63], which seemed to manifest when ICC is high or when the spatial range is large.

In summary, our proposed spatial approach (CRT-SMM) outperformed methods that ignore spatial variability, yielding higher power when $\phi = 3.5$ and showing potential to surpass other methods when $\phi = 1.5$. In addition, FPR assessed type I error control, %RE evaluated variance calibration, coverage probability examined uncertainty validity, and bias and MSE measured estimator accuracy and overall quality. Together, these metrics demonstrated that CRT-SMM excelled in stable and reliable inference.

Sensitivity analyses for different covariance functions and priors for the Gaussian process in CRT-SMM are provided in the Appendices. Table S1 outlines six prior settings based on varying covariance functions and hyperpriors for the spatial parameters ϕ and τ^2 .

For these analyses, we focus on CRT-SMM under the setting with true ICC = 0.05 (corresponding to $\tau^2 = 0.125$) and $\phi = 3.5$. Table S2 summarizes results from 10,000 simulations when the true treatment effects were set as $\theta \in \{0, 0.3, 0.6\}$. The findings demonstrate that CRT-SMM remains robust across different prior specifications.

5 Discussion

We have provided comprehensive methods for CRTs under varying spatial correlations and ICC, highlighting substantial differences in power, FPR, %RE, coverage probability, bias, and MSE. Across 10,000 simulation replications, our findings demonstrate that methods that fail to demonstrate spatial dependency consistently underestimate uncertainty and inflate type I errors. These deficiencies manifest in scenarios where ICC is as high as 0.15 or 0.25 or when spatial range ϕ is as high as 3.5. This spatial range is reasonable for a 4×4 grid where in a real-world, shared environmental or health system factors could impact each individual's response depending on the trial tasks and should be considered through spatial dependencies.

Our model that incorporates individuals' locations to account for spatial heterogeneity offers several benefits. First, it captures geographic variation in outcomes, recognizing that the effect of an intervention on health outcomes may vary spatially due to environmental, socioeconomic, and healthcare access factors. Second, it accounts for spillover effects; for example, in a vaccine trial, herd immunity can arise in groups that received the intervention. Failing to account for spatial dependency may therefore lead to incorrect estimates of treatment effects. Third, it improves efficiency in sample size calculation as understanding spatial correlation allows for more informed cluster size selection, reducing the number of participants needed. Lastly, it supports optimization of randomization and trial site selection.

Our methods can be extended to stepped-wedge designs, in which more clusters are exposed to the intervention toward the end of the study than at its early stage; to crossover designs, in which clusters are randomized sequentially to two or more arms and eventually each cluster receives both arms, serving as its own control for treatment comparisons [14]; and even to randomized control trials that incorporate geocoded participant locations.

Key considerations for designing and analyzing CRTs must be carefully addressed. Compared with individually randomized trials, CRTs typically require larger sample sizes, involve added complexities, and have a greater risk of bias [54]. Nevertheless, despite the belief that CRTs lack precision, Raudenbush (1997) [5] argued that efficient modeling with the use of information at each level, combined with careful choice of covariates and sound planning of the design, can significantly improve the precision of CRTs. Building on this, our demonstration of spatial point process methods for geographical CRTs highlights the potential for broader applications by incorporating spatial methods and integrating not only individual biomarkers but also neighborhood, socioeconomic, and environmental factors into the analytic framework.

Table 1. Scenarios for data generation with a fixed cluster size of $m = 40$, desired treatment effect $\theta = 0.6$, and $\sigma_W^2 = 2.25$, using 16 clusters with a 1:1 allocation ratio.

Scenario	ICC	σ_B^2	τ^2	ϕ	θ
A	0.05	0.125	0.125	1.5	{0-1.4 by 0.1}
B	0.05	0.125	0.125	3.5	{0-1.4 by 0.1}
C	0.15	0.482	0.482	1.5	{0-1.4 by 0.1}
D	0.15	0.482	0.482	3.5	{0-1.4 by 0.1}
E	0.25	1.125	1.125	1.5	{0-1.4 by 0.1}
F	0.25	1.125	1.125	3.5	{0-1.4 by 0.1}

Note: For the decay parameter ϕ , smaller values correspond to faster decay with distance, meaning that points further apart become much less correlated; For spatial variability τ^2 , a larger value means higher spatial heterogeneity, which implies stronger local effects.

Table 2. Posterior mean ($\hat{\theta}$) and standard deviation ($\hat{\sigma}_\theta$) of the treatment effect from 10,000 simulations for true values $\theta = 0, 0.3$, and 0.6 across scenarios.

θ	Scenario	CRT-SMM		CRT-FM-naïve		CRT-FM		CRT-MM		CRT-cluster	
		$\hat{\theta}$	$\hat{\sigma}_\theta$								
0	A	0.00	0.24	0.00	0.12	-0.00	0.38	0.00	0.25	0.00	0.27
	B	-0.00	0.27	0.00	0.14	-0.00	0.39	0.00	0.46	0.00	0.50
	C	0.00	0.48	0.00	0.16	0.01	0.39	0.00	0.66	0.01	0.72
	D	-0.00	0.49	0.02	0.34	0.03	0.41	0.02	1.84	0.02	2.01
	E	-0.02	0.95	-0.04	0.46	-0.03	0.46	-0.04	2.36	-0.04	2.58
	F	0.02	0.96	0.04	1.53	-0.01	0.79	0.01	5.69	-0.00	6.33
0.3	A	0.30	0.24	0.30	0.12	0.26	0.38	0.30	0.25	0.30	0.27
	B	0.30	0.27	0.30	0.14	0.25	0.39	0.30	0.46	0.29	0.50
	C	0.30	0.48	0.30	0.16	0.26	0.39	0.30	0.66	0.30	0.72
	D	0.31	0.49	0.27	0.34	0.23	0.41	0.26	1.83	0.27	2.00
	E	0.30	0.96	0.31	0.46	0.25	0.46	0.29	2.36	0.29	2.58
	F	0.31	0.96	0.31	1.53	0.10	0.79	0.21	5.67	0.17	6.32
0.6	A	0.60	0.24	0.60	0.12	0.51	0.38	0.60	0.25	0.60	0.27
	B	0.60	0.27	0.60	0.14	0.51	0.39	0.60	0.46	0.60	0.50
	C	0.60	0.48	0.60	0.16	0.51	0.39	0.59	0.66	0.59	0.72
	D	0.60	0.49	0.62	0.34	0.54	0.41	0.59	1.84	0.59	2.01
	E	0.60	0.96	0.62	0.46	0.48	0.46	0.58	2.36	0.58	2.59
	F	0.60	0.96	0.54	1.53	0.19	0.8	0.37	5.69	0.32	6.34

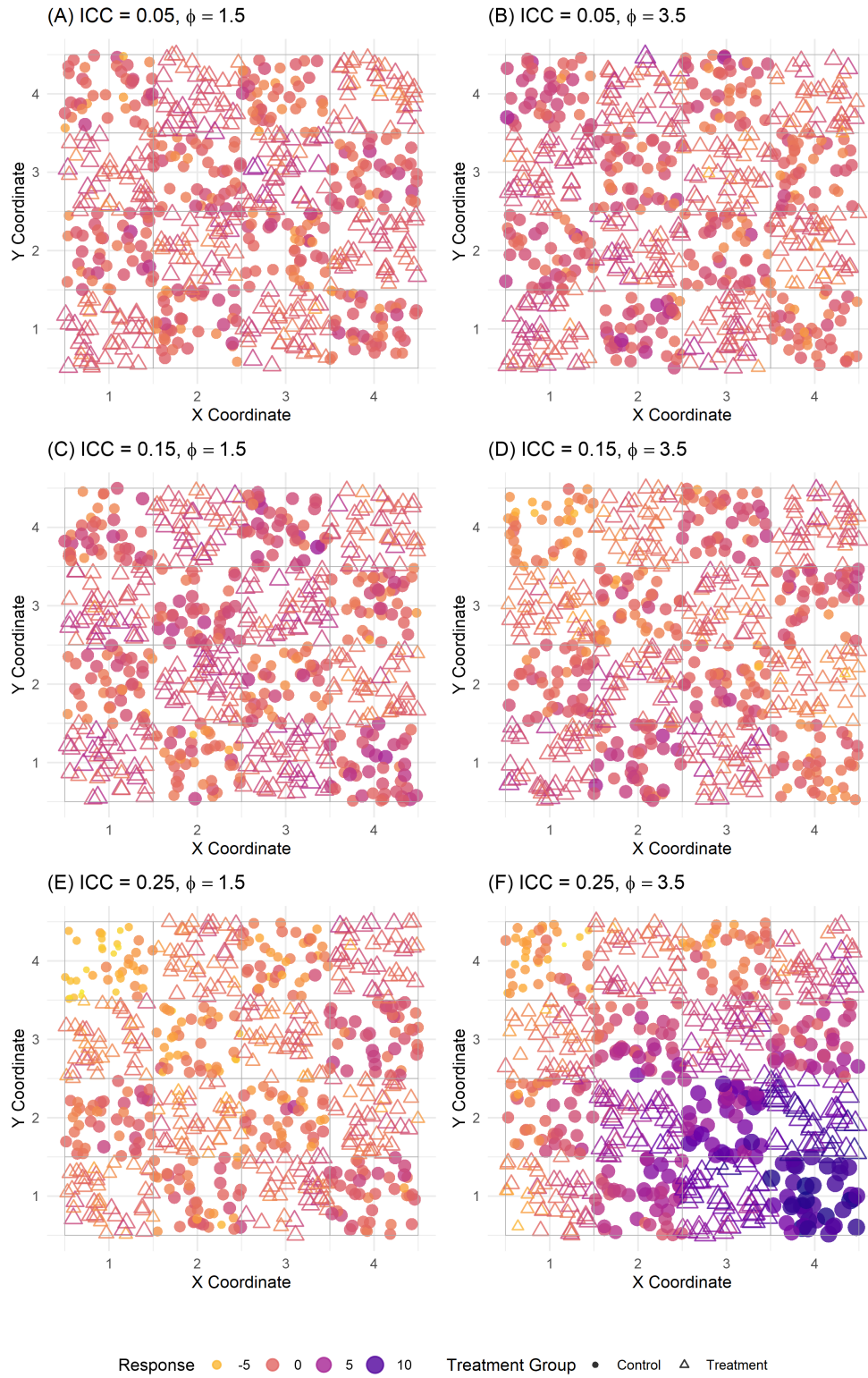


Figure 1. Patient responses from a single simulation replicate with restricted checkerboard structure across scenarios when true $\theta = 0.5$.

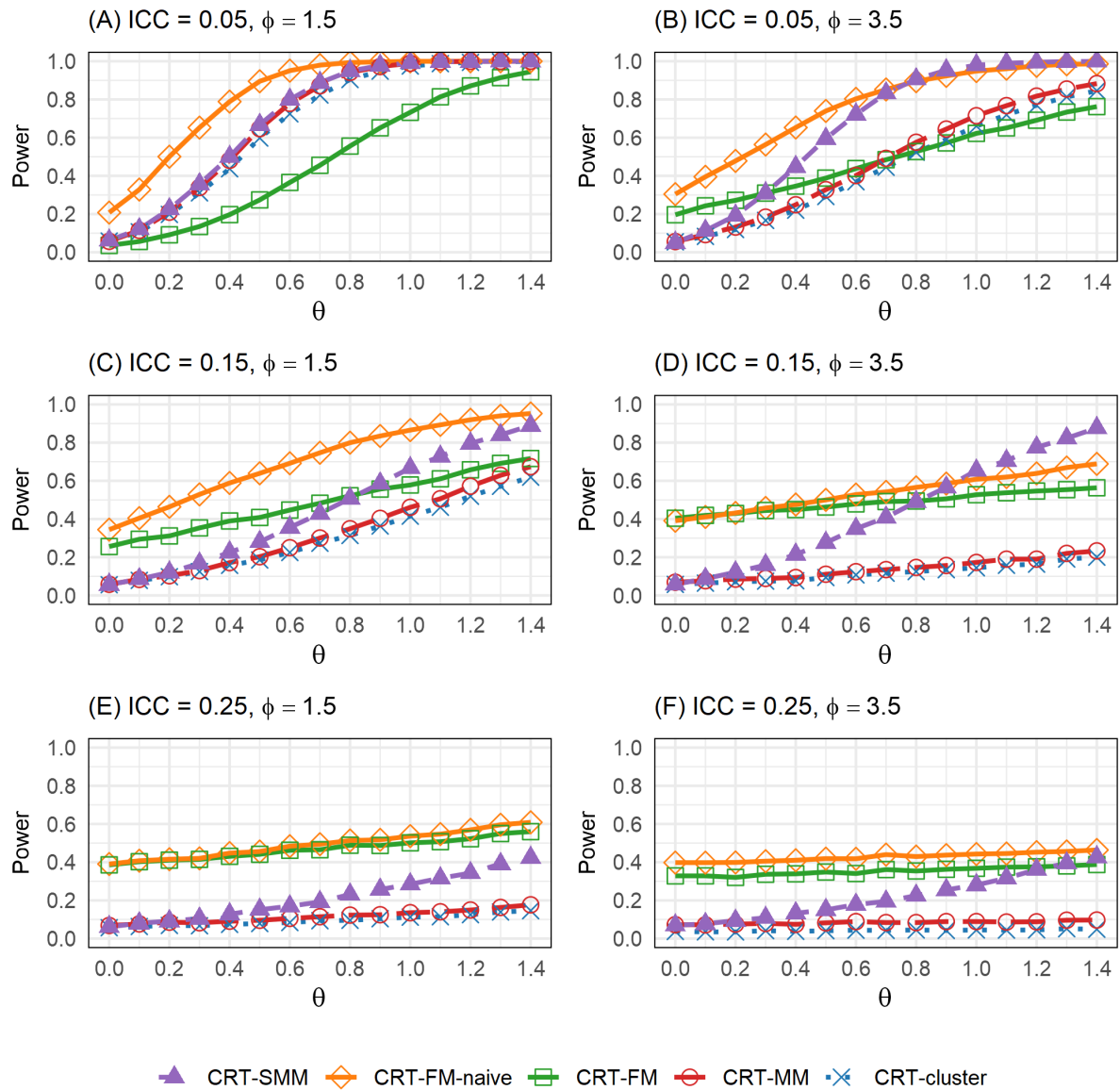


Figure 2. Power curves of 10,000 simulations across true treatment θ 's presented by scenarios. The number of clusters was fixed at 16, as determined by the CRT design calculation corresponding to ICC = 0.05.

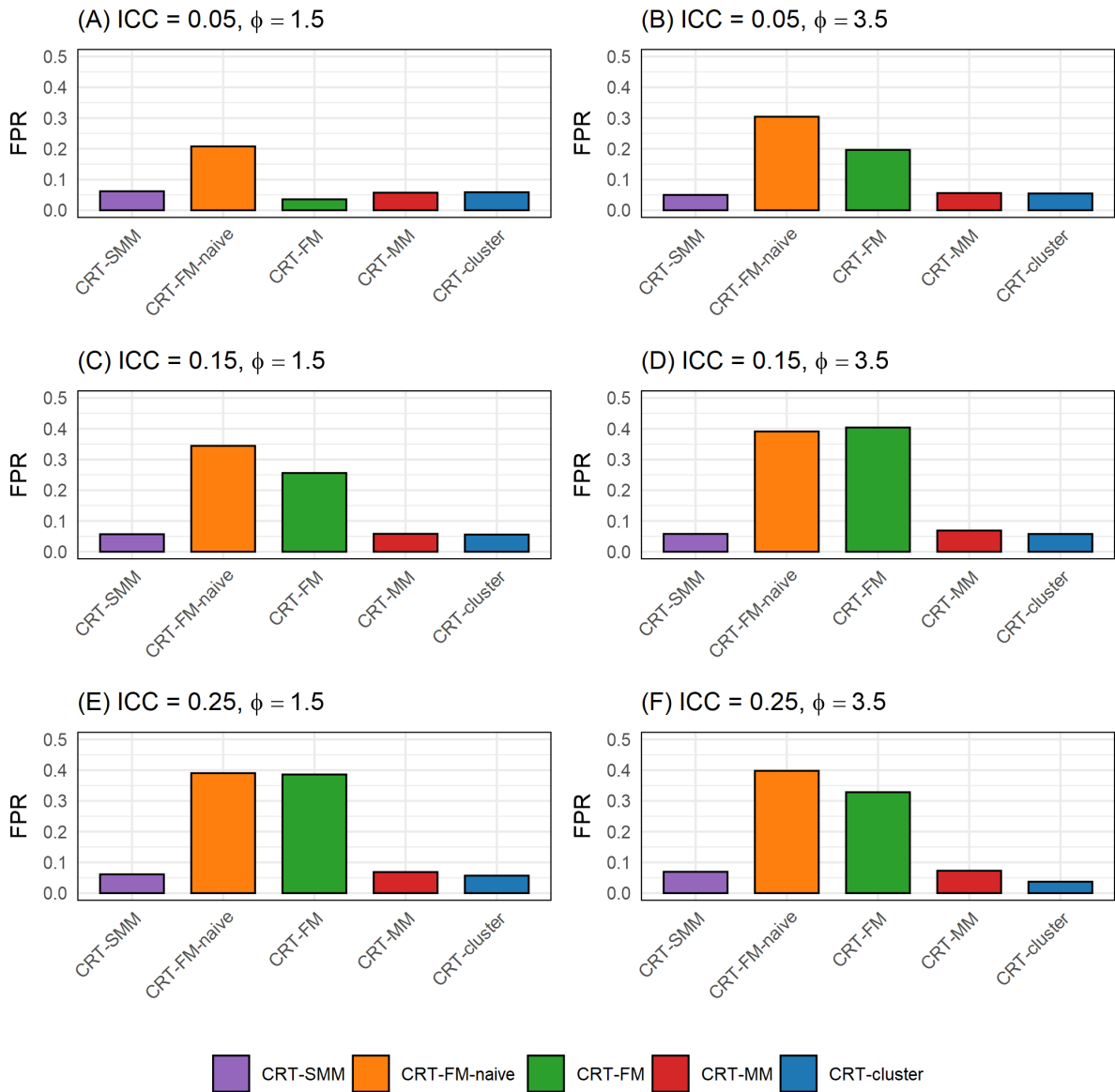


Figure 3. False positive rates (FPRs) of 10,000 simulations across scenarios.

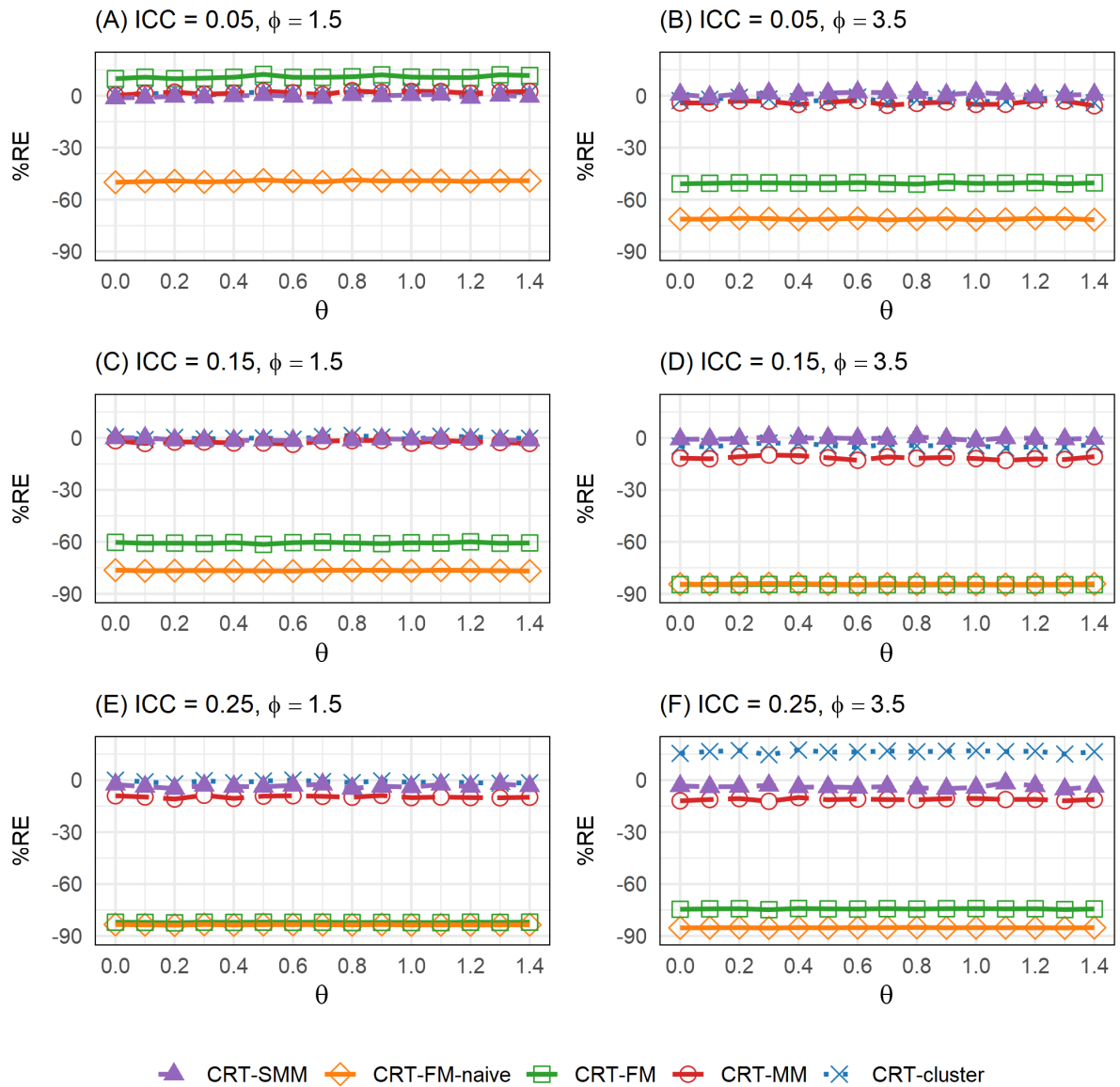


Figure 4. Percent relative error (%RE) of 10,000 simulations across true treatment θ 's presented by scenarios.

Funding

No external funding was received for this study.

Conflict of interest statement

None declared.

Supplementary material

See Supplementary material file.

Data availability

The R code for implementing the proposed method, simulations, and data examples is available at <https://github.com/susanlee505/Spatial-Point-Process-CRT>.

Author's Note

This manuscript has been submitted for consideration in a peer-reviewed journal.

References

1. Schulz, K. F., Altman, D. G. & Moher, D. CONSORT 2010 Statement: Updated Guidelines for Reporting Parallel Group Randomised Trials. *Journal of Pharmacology and Pharmacotherapeutics* **1**, 100–107. ISSN: 0976-500X, 0976-5018. <https://journals.sagepub.com/doi/10.4103/0976-500X.72352> (2010).
2. WHO. *Ethical Issues Related to Study Design for Trials on Therapeutics for Ebola Virus Disease* https://www.who.int/publications/i/item/WHO_HIS_KER_GHE_14.2.
3. Kennedy, S. B. *et al.* Implementation of an Ebola Virus Disease Vaccine Clinical Trial during the Ebola Epidemic in Liberia: Design, Procedures, and Challenges. *Clinical Trials* **13**, 49–56. ISSN: 1740-7745, 1740-7753. <https://journals.sagepub.com/doi/10.1177/1740774515621037> (2016).
4. Kahn, R., Rid, A., Smith, P. G., Eyal, N. & Lipsitch, M. Choices in Vaccine Trial Design in Epidemics of Emerging Infections. *PLOS Medicine* **15**, e1002632. ISSN: 1549-1676. <https://journals.plos.org/plosmedicine/article?id=10.1371/journal.pmed.1002632> (2018).
5. Raudenbush, S. W. Statistical Analysis and Optimal Design for Cluster Randomized Trials. *Statistical Analysis* (1997).
6. Campbell, M. J., Donner, A. & Klar, N. Developments in Cluster Randomized Trials and Statistics in Medicine. *Statistics in Medicine* **26**, 2–19. ISSN: 0277-6715, 1097-0258 (2007).
7. Boulton, C. *et al.* The Effect of Guided Care Teams on the Use of Health Services: Results from a Cluster-Randomized Controlled Trial. *Archives of internal medicine* **171**, 460–466. <https://jamanetwork.com/journals/jamainternalmedicine/article-abstract/226766> (2011).

8. Moher, M. *et al.* Cluster Randomised Controlled Trial to Compare Three Methods of Promoting Secondary Prevention of Coronary Heart Disease in Primary Care. *Bmj* **322**, 1338. <https://www.bmj.com/content/322/7298/1338.abstract> (2001).
9. Benrimoh, D. *et al.* Aifred Health, a Deep Learning Powered Clinical Decision Support System for Mental Health, 251–287 (2018).
10. Tanguay-Sela, M. *et al.* Evaluating the Perceived Utility of an Artificial Intelligence-Powered Clinical Decision Support System for Depression Treatment Using a Simulation Center. *Psychiatry research* **308**, 114336. <https://www.sciencedirect.com/science/article/pii/S0165178121006302> (2022).
11. Borgey, F. *et al.* Effectiveness of an Intervention Campaign on Influenza Vaccination of Professionals in Nursing Homes: A Cluster-Randomized Controlled Trial. *Vaccine* **37**, 1260–1265. <https://www.sciencedirect.com/science/article/pii/S0264410X19301513> (2019).
12. Banerjee, A. V., Duflo, E., Glennerster, R. & Kothari, D. Improving Immunisation Coverage in Rural India: Clustered Randomised Controlled Evaluation of Immunisation Campaigns with and without Incentives. *Bmj* **340**. <https://www.bmj.com/content/340/bmj.c2220.short> (2010).
13. Varma, A. *et al.* Research Protocol of Two Concurrent Cluster-Randomized Trials: Real-life Effect of a CAMPAign with Measles Vaccination (RECAmp-MV) and Real-life Effect of a CAMPAign with Oral Polio Vaccination (RECAmp-OPV) on Mortality and Morbidity among Children in Rural Guinea-Bissau. *BMC Public Health* **19**. ISSN: 1471-2458. <https://bmcpublihealth.biomedcentral.com/articles/10.1186/s12889-019-7813-y> (2019).
14. Lewis, J. A. Statistical Principles for Clinical Trials (ICH E9): An Introductory Note on an International Guideline. *Statistics in Medicine* **18**, 1903–1942. https://odin.mdacc.tmc.edu/~jjlee/clinical_trials2008/lewis,%20ich%20e9,%20stat%20in%20med%201999.pdf (1999).
15. Laird, N. M. & Ware, J. H. Random-Effects Models for Longitudinal Data. *Biometrics*, 963–974. JSTOR: 2529876. <https://www.jstor.org/stable/2529876> (1982).
16. Liang, K.-Y. & Zeger, S. L. Longitudinal Data Analysis Using Generalized Linear Models. *Biometrika* **73**, 13–22 (1986).
17. Hayes, R. J. & Moulton, L. H. *Cluster Randomised Trials: Richard J. Hayes; Lawrence H. Moulton* ISBN: 978-1-58488-816-1 (Chapman & Hall/CRC, Boca Raton, Fla., 2009).
18. Campbell, M. K., Piaggio, G., Elbourne, D. R. & Altman, D. G. Consort 2010 Statement: Extension to Cluster Randomised Trials. *Bmj* **345**. <https://www.bmj.com/content/345/bmj.e5661.abstract> (2012).
19. Spiegelhalter, D. J. Bayesian Methods for Cluster Randomized Trials with Continuous Responses. *Statistics in Medicine* **20**, 435–452. ISSN: 0277-6715, 1097-0258. [https://onlinelibrary.wiley.com/doi/10.1002/1097-0258\(20010215\)20:3<435::AID-SIM804>3.0.CO;2-E](https://onlinelibrary.wiley.com/doi/10.1002/1097-0258(20010215)20:3<435::AID-SIM804>3.0.CO;2-E) (2001).

20. Jones, B. G., Streeter, A. J., Baker, A., Moyeed, R. & Creanor, S. Bayesian Statistics in the Design and Analysis of Cluster Randomised Controlled Trials and Their Reporting Quality: A Methodological Systematic Review. *Systematic Reviews* **10**, 91. ISSN: 2046-4053. <https://doi.org/10.1186/s13643-021-01637-1> (2021).
21. Gimnig, J. E. *et al.* EFFECT OF PERMETHRIN-TREATED BED NETS ON THE SPATIAL DISTRIBUTION OF MALARIA VECTORS IN WESTERN KENYA. *The American Journal of Tropical Medicine and Hygiene* **68**, 115–120. ISSN: 0002-9637. https://www.ajtmh.org/view/journals/tpmd/68/4_suppl/article-p115.xml (2003).
22. Binka, F. N., Indome, F & Smith, T. Impact of Spatial Distribution of Permethrin-Impregnated Bed Nets on Child Mortality in Rural Northern Ghana. *The American Journal of Tropical Medicine and Hygiene* **59**, 80–85. ISSN: 0002-9637. <https://www.ajtmh.org/view/journals/tpmd/59/1/article-p80.xml> (1998).
23. Hawley, W. A. *et al.* Community-wide effects of permethrin-treated bed nets on child mortality and malaria morbidity in western Kenya. *The American Journal of Tropical Medicine and Hygiene* **68**, 121–127. ISSN: 0002-9637. https://www.ajtmh.org/view/journals/tpmd/68/4_suppl/article-p121.xml (2003).
24. Lenhart, A. *et al.* Insecticide-Treated Bednets to Control Dengue Vectors: Preliminary Evidence from a Controlled Trial in Haiti. *Tropical Medicine & International Health* **13**, 56–67. ISSN: 1365-3156. <https://onlinelibrary.wiley.com/doi/abs/10.1111/j.1365-3156.2007.01966.x> (2008).
25. Freeman, M. C. *et al.* Assessing the Impact of a School-based Water Treatment, Hygiene and Sanitation Programme on Pupil Absence in Nyanza Province, Kenya: A Cluster-randomized Trial. *Tropical Medicine & International Health* **17**, 380–391. ISSN: 1360-2276, 1365-3156 (2012).
26. Alexander, N. D. *et al.* Spatial Variation of Anopheles-transmitted *Wuchereria Bancrofti* and *Plasmodium Falciparum* Infection Densities in Papua New Guinea. *Filaria Journal* **2**, 14. ISSN: 1475-2883. <https://filariajournal.biomedcentral.com/articles/10.1186/1475-2883-2-14> (2003).
27. Kroeger, A. *et al.* Effective Control of Dengue Vectors with Curtains and Water Container Covers Treated with Insecticide in Mexico and Venezuela: Cluster Randomised Trials. *BMJ : British Medical Journal* **332**, 1247–1252. ISSN: 0959-8138. PMID: 16735334. <https://www.ncbi.nlm.nih.gov/pmc/articles/PMC1471956/> (2006).
28. Ali, M *et al.* Geographic Analysis of Vaccine Uptake in a Cluster-Randomized Controlled Trial in Hue, Vietnam. *Health & Place* **13**, 577–587. ISSN: 13538292. <https://linkinghub.elsevier.com/retrieve/pii/S1353829206000517> (2007).
29. Miguel, E. & Kremer, M. Worms: Identifying Impacts on Education and Health in the Presence of Treatment Externalities (2004).

30. Chao, D. L. *et al.* The Contribution of Neighbours to an Individual's Risk of Typhoid Outcome. *Epidemiology and Infection* **143**, 3520–3527. ISSN: 0950-2688, 1469-4409. https://www.cambridge.org/core/product/identifier/S0950268815000692/type/journal_article (2015).
31. John, T. J. & Samuel, R. Herd Immunity and Herd Effect: New Insights and Definitions. *European Journal of Epidemiology* **16**, 601–606. ISSN: 0393-2990, 1573-7284. <https://link.springer.com/10.1023/A:1007626510002> (2000).
32. Zhu, G. & Stewart, K. Space-Time Relationships between COVID-19 Vaccinations and Human Mobility Patterns in the United States. *Applied Geography* **159**, 103086. ISSN: 0143-6228 (2023).
33. Jarvis, C., Di Tanna, G. L., Lewis, D., Alexander, N. & Edmunds, W. J. Spatial Analysis of Cluster Randomised Trials: A Systematic Review of Analysis Methods. *Emerging Themes in Epidemiology* **14**, 12. ISSN: 1742-7622. <https://doi.org/10.1186/s12982-017-0066-2> (2017).
34. Barrios, T., Diamond, R., Imbens, G. W. & Kolesár, M. Clustering, Spatial Correlations, and Randomization Inference. *Journal of the American Statistical Association* **107**, 578–591. ISSN: 0162-1459, 1537-274X (2012).
35. Baylis, K. & Ham, A. How Important Is Spatial Correlation in Randomized Controlled Trials? (2015).
36. Guo, B. & Zang, Y. A Bayesian Adaptive Phase II Clinical Trial Design Accounting for Spatial Variation. *Statistical Methods in Medical Research* **28**, 3187–3204. ISSN: 0962-2802, 1477-0334. <https://journals.sagepub.com/doi/10.1177/0962280218797149> (2019).
37. Banerjee, S., Carlin, B. P. & Gelfand, A. E. *Hierarchical Modeling and Analysis for Spatial Data* 23–32. <https://www.taylorfrancis.com/books/mono/10.1201/9780203487808/hierarchical-modeling-analysis-spatial-data-sudipto-banerjee-sudipto-banerjee-bradley-carlin-alan-gelfand> (Chapman and Hall/CRC, 2003).
38. Blangiardo, M. & Cameletti, M. *Spatial and Spatio-Temporal Bayesian Models with R-INLA* 173–229. ISBN: 978-1-118-95019-7 978-1-118-95021-0 (John Wiley and Sons, Inc, Chichester, West Sussex, 2015).
39. Wikle, C. K., Zammit Mangion, A. & Cressie, N. A. C. *Spatio-Temporal Statistics with R* 1 p. ISBN: 978-1-138-71113-6 978-1-351-76972-3 978-0-429-64714-7 978-0-429-64450-4 978-0-429-64978-3 (CRC Press, Boca Raton London New York, 2019).
40. Eldridge, S. M., Ukoumunne, O. C. & Carlin, J. B. The Intra-Cluster Correlation Coefficient in Cluster Randomized Trials: A Review of Definitions. *International Statistical Review* **77**, 378–394. ISSN: 0306-7734, 1751-5823. <https://onlinelibrary.wiley.com/doi/10.1111/j.1751-5823.2009.00092.x> (2009).
41. Gelfand, A. E. & Schliep, E. M. Spatial Statistics and Gaussian Processes: A Beautiful Marriage. *Spatial Statistics* **18**. ISSN: 22116753 (2016).

42. Rue, H., Martino, S. & Chopin, N. Approximate Bayesian Inference for Latent Gaussian Models by Using Integrated Nested Laplace Approximations. *Journal of the Royal Statistical Society Series B: Statistical Methodology* **71**, 319–392. <https://academic.oup.com/jrsssb/article-abstract/71/2/319/7092907> (2009).
43. Lindgren, F., Rue, H. & Lindström, J. An Explicit Link between Gaussian Fields and Gaussian Markov Random Fields: The Stochastic Partial Differential Equation Approach. *Journal of the Royal Statistical Society Series B: Statistical Methodology* **73**, 423–498. <https://academic.oup.com/jrsssb/article-abstract/73/4/423/7034732> (2011).
44. Raab, G. M. & Butcher, I. Balance in Cluster Randomized Trials. *Statistics in Medicine* **20**, 351–365. ISSN: 0277-6715, 1097-0258. [https://onlinelibrary.wiley.com/doi/10.1002/1097-0258\(20010215\)20:3<351::AID-SIM797>3.0.CO;2-C](https://onlinelibrary.wiley.com/doi/10.1002/1097-0258(20010215)20:3<351::AID-SIM797>3.0.CO;2-C) (2001).
45. Moulton, L. H. Covariate-Based Constrained Randomization of Group-Randomized Trials. *Clinical Trials* **1**, 297–305. ISSN: 1740-7745, 1740-7753. <https://journals.sagepub.com/doi/10.1191/1740774504cn024oa> (2004).
46. Snaveley, A. C. *et al.* Intracluster Correlation Coefficients from Cluster Randomized Trials Conducted within the NCI Community Oncology Research Program (NCORP). *JNCI Monographs* **2025**, 65–72. ISSN: 1052-6773, 1745-6614 (2025).
47. Campbell, M. K., Mollison, J. & Grimshaw, J. M. Cluster Trials in Implementation Research: Estimation of Intracluster Correlation Coefficients and Sample Size. *Statistics in Medicine* **20**, 391–399. ISSN: 0277-6715, 1097-0258 (2001).
48. Adams, G. *et al.* Patterns of Intra-Cluster Correlation from Primary Care Research to Inform Study Design and Analysis. *Journal of Clinical Epidemiology* **57**, 785–794 (2004).
49. Elley, C. R., Kerse, N., Chondros, P. & Robinson, E. Intraclass Correlation Coefficients from Three Cluster Randomised Controlled Trials in Primary and Residential Health Care. *Australian and New Zealand Journal of Public Health* **29**, 461–467 (2005).
50. Murray, D. M. *et al.* Intraclass Correlation among Common Measures of Adolescent Smoking: Estimates, Correlates, and Applications in Smoking Prevention Studies. *American Journal of Epidemiology* **140**, 1038–1050 (1994).
51. Murray, D. M. & Short, B. Intraclass Correlation among Measures Related to Alcohol Use by Young Adults: Estimates, Correlates and Applications in Intervention Studies. *Journal of Studies on Alcohol* **56**, 681–694. ISSN: 0096-882X, 1934-2683. <https://www.jsad.com/doi/10.15288/jsa.1995.56.681> (1995).
52. Taljaard, M. *et al.* Inadequate Reporting of Research Ethics Review and Informed Consent in Cluster Randomised Trials: Review of Random Sample of Published Trials. *Bmj* **342**. <https://www.bmj.com/content/342/bmj.d2496.abstract> (2011).

53. Arnup, S. J., McKenzie, J. E., Hemming, K., Pilcher, D. & Forbes, A. B. Understanding the Cluster Randomised Crossover Design: A Graphical Illustration of the Components of Variation and a Sample Size Tutorial. *Trials* **18**, 381. ISSN: 1745-6215. <https://doi.org/10.1186/s13063-017-2113-2> (2017).
54. Hemming, K. & Taljaard, M. Key Considerations for Designing, Conducting and Analysing a Cluster Randomized Trial. *International Journal of Epidemiology* **52**, 1648–1658. ISSN: 0300-5771. <https://doi.org/10.1093/ije/dyad064> (2023).
55. Simpson, D., Rue, H., Riebler, A., Martins, T. G. & Sørbye, S. H. Penalising Model Component Complexity: A Principled, Practical Approach to Constructing Priors. <https://projecteuclid.org/journals/statistical-science/volume-32/issue-1/Penalising-Model-Component-Complexity--A-Principled-Practical-Approach-to/10.1214/16-STS576.short> (2017).
56. Kullback, S. & Leibler, R. A. On Information and Sufficiency. *The Annals of Mathematical Statistics* **22**, 79–86. JSTOR: 2236703 (1951).
57. Kat, C.-J. & Els, P. S. Validation Metric Based on Relative Error. *Mathematical and Computer Modelling of Dynamical Systems* **18**, 487–520. ISSN: 1387-3954, 1744-5051. <http://www.tandfonline.com/doi/abs/10.1080/13873954.2012.663392> (2012).
58. Agresti, A. & Kateri, M. in *International Encyclopedia of Statistical Science* (ed Lovric, M.) 289–291 (Springer Berlin Heidelberg, Berlin, Heidelberg, 2011). ISBN: 978-3-642-04897-5 978-3-642-04898-2.
59. Bartels, B. L. Beyond "Fixed Versus Random Effects": A Framework for Improving Substantive and Statistical Analysis of Panel, Time-series Cross-sectional, and Multilevel Data. *The Society for Political Methodology* **9** (2008).
60. Tutz, G. & Oelker, M.-R. Modeling Clustered Heterogeneity: Fixed Effects, Random Effects and Mixtures. *International Statistical Review* (2017).
61. R Core Team. *R: A Language and Environment for Statistical Computing* R Foundation for Statistical Computing (Vienna, Austria, 2025). <https://www.R-project.org/>.
62. Hsiao, C. *Analysis of Panel Data* **64**. <https://books.google.co.kr/books?hl=en&lr=&id=DHtrEAAAQBAJ&oi=fnd&pg=PR13&dq=Analysis+of+Panel+Data&ots=QThdsTVBr1&sig=KbqA9jPntHW7iHmMSfjOTp4Lxp0> (Cambridge university press, 2022).
63. Skrondal, A. & Rabe-Hesketh, S. *Generalized Latent Variable Modeling: Multilevel, Longitudinal, and Structural Equation Models* <https://www.taylorfrancis.com/books/mono/10.1201/9780203489437/generalized-latent-variable-modeling-anders-skrondal-sophia-rabe-hesketh> (Chapman and Hall/CRC, 2004).